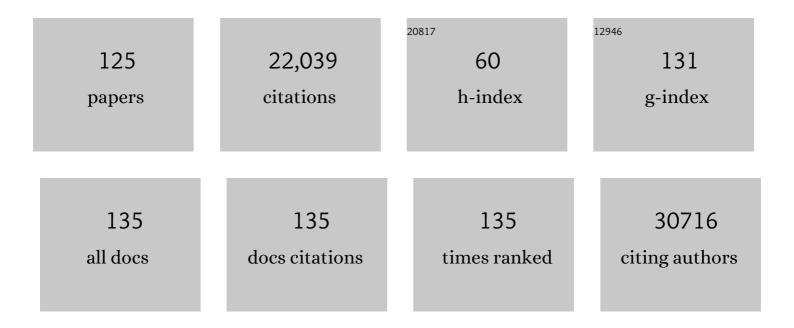
## Hyeon S Shin

List of Publications by Year in descending order

Source: https://exaly.com/author-pdf/7418049/publications.pdf Version: 2024-02-01



#	Article	IF	CITATIONS
1	The chemistry of two-dimensional layered transition metal dichalcogenide nanosheets. Nature Chemistry, 2013, 5, 263-275.	13.6	8,051
2	High-quality graphene via microwave reduction of solution-exfoliated graphene oxide. Science, 2016, 353, 1413-1416.	12.6	670
3	A Ceneral Approach to Preferential Formation of Active Fe–N <sub><i>x</i></sub> Sites in Fe–N/C Electrocatalysts for Efficient Oxygen Reduction Reaction. Journal of the American Chemical Society, 2016, 138, 15046-15056.	13.7	663
4	High yield exfoliation of two-dimensional chalcogenides using sodium naphthalenide. Nature Communications, 2014, 5, 2995.	12.8	655
5	Low-dimensional catalysts for hydrogen evolution and CO2 reduction. Nature Reviews Chemistry, 2018, 2, .	30.2	631
6	Resonantly hybridized excitons in moiré superlattices in van der Waals heterostructures. Nature, 2019, 567, 81-86.	27.8	621
7	Multicomponent electrocatalyst with ultralow Pt loading and high hydrogen evolution activity. Nature Energy, 2018, 3, 773-782.	39.5	542
8	Twoâ€Dimensional Hybrid Nanosheets of Tungsten Disulfide and Reduced Graphene Oxide as Catalysts for Enhanced Hydrogen Evolution. Angewandte Chemie - International Edition, 2013, 52, 13751-13754.	13.8	474
9	Growth of High-Crystalline, Single-Layer Hexagonal Boron Nitride on Recyclable Platinum Foil. Nano Letters, 2013, 13, 1834-1839.	9.1	336
10	Interaction between Metal and Graphene: Dependence on the Layer Number of Graphene. ACS Nano, 2011, 5, 608-612.	14.6	324
11	Efficient Hydrogen Evolution Reaction Catalysis in Alkaline Media by Allâ€inâ€One MoS <sub>2</sub> with Multifunctional Active Sites. Advanced Materials, 2018, 30, e1707105.	21.0	321
12	Seamless Stitching of Graphene Domains on Polished Copper (111) Foil. Advanced Materials, 2015, 27, 1376-1382.	21.0	314
13	Transparent, Flexible Conducting Hybrid Multilayer Thin Films of Multiwalled Carbon Nanotubes with Graphene Nanosheets. ACS Nano, 2010, 4, 3861-3868.	14.6	313
14	Synthesis and Characterization of Patronite Form of Vanadium Sulfide on Graphitic Layer. Journal of the American Chemical Society, 2013, 135, 8720-8725.	13.7	300
15	Effects of Surface Anchoring Groups (Carboxylate vs Phosphonate) in Ruthenium-Complex-Sensitized TiO2 on Visible Light Reactivity in Aqueous Suspensions. Journal of Physical Chemistry B, 2004, 108, 14093-14101.	2.6	281
16	Ultrahigh-current-density niobium disulfide catalysts for hydrogen evolution. Nature Materials, 2019, 18, 1309-1314.	27.5	280
17	Recent advances in layered transition metal dichalcogenides for hydrogen evolution reaction. Journal of Materials Chemistry A, 2014, 2, 5979-5985.	10.3	258
18	Mechanism of growth of colloidal silver nanoparticles stabilized by polyvinyl pyrrolidone in 13-irradiated silver nitrate solution, Journal of Colloid and Interface Science, 2004, 274, 89-94	9.4	231

#	Article	IF	CITATIONS
19	Probing Evolution of Twist-Angle-Dependent Interlayer Excitons in MoSe <sub>2</sub> /WSe <sub>2</sub> van der Waals Heterostructures. ACS Nano, 2017, 11, 4041-4050.	14.6	227
20	Highâ€Performance Hydrogen Evolution by Ru Single Atoms and Nitridedâ€Ru Nanoparticles Implanted on Nâ€Doped Graphitic Sheet. Advanced Energy Materials, 2019, 9, 1900931.	19.5	224
21	Monolayer-Precision Synthesis of Molybdenum Sulfide Nanoparticles and Their Nanoscale Size Effects in the Hydrogen Evolution Reaction. ACS Nano, 2015, 9, 3728-3739.	14.6	201
22	Poly(vinyl alcohol) Reinforced and Toughened with Poly(dopamine)-Treated Graphene Oxide, and Its Use for Humidity Sensing. ACS Nano, 2014, 8, 6739-6747.	14.6	197
23	Highly controllable transparent and conducting thin films using layer-by-layer assembly of oppositely charged reduced graphene oxides. Journal of Materials Chemistry, 2011, 21, 3438-3442.	6.7	194
24	Monolayer optical memory cells based on artificial trap-mediated charge storage and release. Nature Communications, 2017, 8, 14734.	12.8	184
25	Oxidation Resistance of Iron and Copper Foils Coated with Reduced Graphene Oxide Multilayers. ACS Nano, 2012, 6, 7763-7769.	14.6	175
26	Ultralow-dielectric-constant amorphous boron nitride. Nature, 2020, 582, 511-514.	27.8	173
27	Strain-Mediated Interlayer Coupling Effects on the Excitonic Behaviors in an Epitaxially Grown MoS <sub>2</sub> /WS <sub>2</sub> van der Waals Heterobilayer. Nano Letters, 2017, 17, 5634-5640.	9.1	169
28	Wafer-Scale and Wrinkle-Free Epitaxial Growth of Single-Orientated Multilayer Hexagonal Boron Nitride on Sapphire. Nano Letters, 2016, 16, 3360-3366.	9.1	167
29	Molecular Beam Epitaxy of Highly Crystalline Monolayer Molybdenum Disulfide on Hexagonal Boron Nitride. Journal of the American Chemical Society, 2017, 139, 9392-9400.	13.7	167
30	Graphene oxide nanopaint. Carbon, 2014, 72, 328-337.	10.3	163
31	Effects of nanofluids containing graphene/graphene-oxide nanosheets on critical heat flux. Applied Physics Letters, 2010, 97, .	3.3	162
32	Flexible Thermochromic Window Based on Hybridized VO <sub>2</sub> /Graphene. ACS Nano, 2013, 7, 5769-5776.	14.6	154
33	Surfaceâ€Enhanced Raman Scattering of Single―and Few‣ayer Graphene by the Deposition of Gold Nanoparticles. Chemistry - A European Journal, 2011, 17, 2381-2387.	3.3	133
34	Chemical Vapor Deposition of Highâ€Quality Largeâ€Sized MoS <sub>2</sub> Crystals on Silicon Dioxide Substrates. Advanced Science, 2016, 3, 1500033.	11.2	128
35	Highly Efficient Polymer Light-Emitting Diodes Using Graphene Oxide as a Hole Transport Layer. ACS Nano, 2012, 6, 2984-2991.	14.6	127
36	Multiple Redox Modes in the Reversible Lithiation of High-Capacity, Peierls-Distorted Vanadium Sulfide. Journal of the American Chemical Society, 2015, 137, 8499-8508.	13.7	127

#	Article	IF	CITATIONS
37	Lithium reaction mechanism and high rate capability of VS <sub>4</sub> –graphene nanocomposite as an anode material for lithium batteries. Journal of Materials Chemistry A, 2014, 2, 10847-10853.	10.3	118
38	Thermodynamically Stable Synthesis of Large‣cale and Highly Crystalline Transition Metal Dichalcogenide Monolayers and their Unipolar n–n Heterojunction Devices. Advanced Materials, 2017, 29, 1702206.	21.0	116
39	High-yield production of mono- or few-layer transition metal dichalcogenide nanosheets by an electrochemical lithium ion intercalation-based exfoliation method. Nature Protocols, 2022, 17, 358-377.	12.0	100
40	Large-Area Graphene Films by Simple Solution Casting of Edge-Selectively Functionalized Graphite. ACS Nano, 2011, 5, 4974-4980.	14.6	98
41	Epitaxial single-crystal hexagonal boron nitride multilayers on Ni (111). Nature, 2022, 606, 88-93.	27.8	97
42	Stacking of Two-Dimensional Materials in Lateral and Vertical Directions. Chemistry of Materials, 2014, 26, 4891-4903.	6.7	96
43	Chemical and size effects of nanocomposites of silver and polyvinyl pyrrolidone determined by X-ray photoemission spectroscopy. Chemical Physics Letters, 2004, 383, 418-422.	2.6	94
44	Spatially Resolved Spontaneous Reactivity of Diazonium Salt on Edge and Basal Plane of Graphene without Surfactant and Its Doping Effect. Langmuir, 2010, 26, 12278-12284.	3.5	92
45	Freeze-dried WS2 composites with low content of graphene as high-rate lithium storage materials. Journal of Materials Chemistry A, 2013, 1, 14548.	10.3	89
46	Highly Selective Synthesis of C <sub>60</sub> Disks on Graphite Substrate by a Vapor–Solid Process. Angewandte Chemie - International Edition, 2008, 47, 693-696.	13.8	88
47	Reversibly Light-Modulated Dirac Point of Graphene Functionalized with Spiropyran. ACS Nano, 2012, 6, 9207-9213.	14.6	85
48	Epoxy to Carbonyl Group Conversion in Graphene Oxide Thin Films: Effect on Structural and Luminescent Characteristics. Journal of Physical Chemistry C, 2012, 116, 19010-19017.	3.1	83
49	Unveiling Surface Redox Charge Storage of Interacting Two-Dimensional Heteronanosheets in Hierarchical Architectures. Nano Letters, 2015, 15, 2269-2277.	9.1	80
50	Imaging of Interlayer Coupling in van der Waals Heterostructures Using a Bright-Field Optical Microscope. Nano Letters, 2017, 17, 5342-5349.	9.1	74
51	Hierarchically assembled tubular shell-core-shell heterostructure of hybrid transition metal chalcogenides for high-performance supercapacitors with ultrahigh cyclability. Nano Energy, 2017, 37, 15-23.	16.0	72
52	Highly stable 3D porous heterostructures with hierarchically-coordinated octahedral transition metals for enhanced performance supercapacitors. Nano Energy, 2017, 39, 337-345.	16.0	72
53	Phase-engineered transition-metal dichalcogenides for energy and electronics. MRS Bulletin, 2015, 40, 585-591.	3.5	71
54	Prevention of Transition Metal Dichalcogenide Photodegradation by Encapsulation with h-BN Layers. ACS Nano, 2016, 10, 8973-8979.	14.6	70

#	Article	IF	CITATIONS
55	Modulation of Cu and Rh single-atoms and nanoparticles for high-performance hydrogen evolution activity in acidic media. Journal of Materials Chemistry A, 2021, 9, 10326-10334.	10.3	70
56	Support-Free Transfer of Ultrasmooth Graphene Films Facilitated by Self-Assembled Monolayers for Electronic Devices and Patterns. ACS Nano, 2016, 10, 1404-1410.	14.6	69
57	Large-Scale Graphene Micropatterns via Self-Assembly-Mediated Process for Flexible Device Application. Nano Letters, 2012, 12, 743-748.	9.1	68
58	New Approach to Generalized Two-Dimensional Correlation Spectroscopy. 1: Combination of Principal Component Analysis and Two-Dimensional Correlation Spectroscopy. Applied Spectroscopy, 2002, 56, 1562-1567.	2.2	65
59	Hexagonal Boron Nitride/Au Substrate for Manipulating Surface Plasmon and Enhancing Capability of Surface-Enhanced Raman Spectroscopy. ACS Nano, 2016, 10, 11156-11162.	14.6	64
60	Reduced Graphene Oxide (rGO)-Wrapped Fullerene (C <sub>60</sub> ) Wires. ACS Nano, 2011, 5, 8365-8371.	14.6	63
61	Atomic-scale dynamics of triangular hole growth in monolayer hexagonal boron nitride under electron irradiation. Nanoscale, 2015, 7, 10600-10605.	5.6	63
62	AA′-Stacked Trilayer Hexagonal Boron Nitride Membrane for Proton Exchange Membrane Fuel Cells. ACS Nano, 2018, 12, 10764-10771.	14.6	55
63	Layered material platform for surface plasmon resonance biosensing. Scientific Reports, 2019, 9, 20286.	3.3	55
64	Spontaneous Formation of Transition-Metal Nanoparticles on Single-Walled Carbon Nanotubes Anchored with Conjugated Molecules. Small, 2005, 1, 975-979.	10.0	54
65	Recent Developments in Synthesis and Photocatalytic Applications of Carbon Dots. Catalysts, 2020, 10, 320.	3.5	54
66	Glass Transition Temperature and Conformational Changes of Poly(methyl methacrylate) Thin Films Determined by a Two-Dimensional Map Representation of Temperature-Dependent Reflectionâ~'Absorption FTIR Spectra. Langmuir, 2002, 18, 5953-5958.	3.5	52
67	Catalyst-Free Synthesis of Si-SiO <sub><i>x</i></sub> Core-Shell Nanowire Anodes for High-Rate and High-Capacity Lithium-Ion Batteries. ACS Applied Materials & Interfaces, 2014, 6, 6340-6345.	8.0	52
68	Catalytic Conversion of Hexagonal Boron Nitride to Graphene for In-Plane Heterostructures. Nano Letters, 2015, 15, 4769-4775.	9.1	52
69	Chemical Vapor-Deposited Hexagonal Boron Nitride as a Scalable Template for High-Performance Organic Field-Effect Transistors. Chemistry of Materials, 2017, 29, 2341-2347.	6.7	52
70	Direct Epitaxial Synthesis of Selective Two-Dimensional Lateral Heterostructures. ACS Nano, 2019, 13, 13047-13055.	14.6	52
71	VS2/rGO hybrid nanosheets prepared by annealing of VS4/rGO. Journal of Solid State Chemistry, 2015, 224, 82-87.	2.9	46
72	Surface functionalization-induced photoresponse characteristics of monolayer MoS <sub>2</sub> for fast flexible photodetectors. Nanoscale, 2019, 11, 4726-4734.	5.6	44

#	Article	IF	CITATIONS
73	Substrate and buffer layer effect on the structural and optical properties of graphene oxide thin films. RSC Advances, 2013, 3, 5926.	3.6	43
74	Synthesis and structure of two-dimensional transition-metal dichalcogenides. MRS Bulletin, 2015, 40, 566-576.	3.5	43
75	Planar and van der Waals heterostructures for vertical tunnelling single electron transistors. Nature Communications, 2019, 10, 230.	12.8	43
76	Characterization of Transition Temperatures of a Langmuir—Blodgett Film of Poly(tert-butyl) Tj ETQqO O O rgBT Applied Spectroscopy, 2002, 56, 1568-1574.	/Overlocl 2.2	۱0 Tf 50 62 42
77	Enhanced optical response of hybridized VO2/graphene films. Nanoscale, 2013, 5, 2632.	5.6	36
78	Three-dimensional pillared metallomacrocycle–graphene frameworks with tunable micro- and mesoporosity. Journal of Materials Chemistry A, 2013, 1, 8432.	10.3	32
79	Evidence of Local Commensurate State with Lattice Match of Graphene on Hexagonal Boron Nitride. ACS Nano, 2017, 11, 7084-7090.	14.6	31
80	Mosaic-like Monolayer of Graphene Oxide Sheets Decorated with Tetrabutylammonium Ions. ACS Nano, 2013, 7, 8082-8088.	14.6	30
81	Nafion-Mediated Liquid-Phase Exfoliation of Transition Metal Dichalcogenides and Direct Application in Hydrogen Evolution Reaction. Chemistry of Materials, 2018, 30, 4658-4666.	6.7	30
82	Proton conductivity of a hexagonal boron nitride membrane and its energy applications. Journal of Materials Chemistry A, 2020, 8, 2898-2912.	10.3	27
83	Structural Comparison of Langmuirâ`'Blodgett and Spin-Coated Films of Poly(tert-butyl methacrylate) by External Reflection FTIR Spectroscopy and Two-Dimensional Correlation Analysis. Langmuir, 2002, 18, 5523-5528.	3.5	26
84	Facile Method for rGO Field Effect Transistor: Selective Adsorption of rGO on SAMâ€Treated Gold Electrode by Electrostatic Attraction. Advanced Materials, 2012, 24, 2299-2303.	21.0	26
85	Selective synthesis of pure cobalt disulfide on reduced graphene oxide sheets and its high electrocatalytic activity for hydrogen evolution reaction. Nano Convergence, 2016, 3, 5.	12.1	25
86	General Colloidal Synthesis of Transition-Metal Disulfide Nanomaterials as Electrocatalysts for Hydrogen Evolution Reaction. ACS Applied Materials & Interfaces, 2020, 12, 13148-13155.	8.0	25
87	Study of Cooling Rate on the Growth of Graphene via Chemical Vapor Deposition. Chemistry of Materials, 2017, 29, 4202-4208.	6.7	24
88	Direct patterning of silver colloids by microcontact printing: possibility as SERS substrate array. Vibrational Spectroscopy, 2002, 29, 79-82.	2.2	23
89	Electrochemical and electrocatalytic reaction characteristics of boron-incorporated graphene <i>via</i> Âa simple spin-on dopant process. Journal of Materials Chemistry A, 2018, 6, 7351-7356.	10.3	23
90	Rapid synthesis of graphene by chemical vapor deposition using liquefied petroleum gas as precursor. Carbon, 2019, 145, 462-469.	10.3	23

#	Article	IF	CITATIONS
91	Blue emission at atomically sharp 1D heterojunctions between graphene and h-BN. Nature Communications, 2020, 11, 5359.	12.8	23
92	Hydrogenation of monolayer molybdenum diselenide via hydrogen plasma treatment. Journal of Materials Chemistry C, 2017, 5, 11294-11300.	5.5	20
93	Large area chemical vapour deposition grown transition metal dichalcogenide monolayers automatically characterized through photoluminescence imaging. Npj 2D Materials and Applications, 2020, 4, .	7.9	20
94	Vertically oriented MoS <sub>2</sub> /WS <sub>2</sub> heterostructures on reduced graphene oxide sheets as electrocatalysts for hydrogen evolution reaction. Materials Chemistry Frontiers, 2021, 5, 3396-3403.	5.9	20
95	Chalcogenide solution-mediated activation protocol for scalable and ultrafast synthesis of single-crystalline 1-D copper sulfide for supercapacitors. Journal of Materials Chemistry A, 2019, 7, 2529-2535.	10.3	19
96	Large-scale patterning by the roll-based evaporation-induced self-assembly. Journal of Materials Chemistry, 2012, 22, 22844.	6.7	18
97	2D materials-based photoelectrochemical cells: Combination of transition metal dichalcogenides and reduced graphene oxide for efficient charge transfer. FlatChem, 2017, 4, 54-60.	5.6	18
98	"Fingertip―Guided Noncovalent Functionalization of Carbon Nanotubes by Dendrons. Langmuir, 2007, 23, 11373-11376.	3.5	17
99	Lithium Ions Intercalated into Pyrene-Functionalized Carbon Nanotubes and Their Mass Transport:Â A Chemical Route to Carbon Nanotube Schottky Diode. Journal of the American Chemical Society, 2008, 130, 2160-2161.	13.7	17
100	Transition temperatures and molecular structures of poly(methyl methacrylate) thin films by principal component analysis: comparison of isotactic and syndiotactic poly(methyl methacrylate). Vibrational Spectroscopy, 2005, 37, 69-76.	2.2	16
101	Two-Dimensional Gradient Mapping Technique Useful for Detailed Spectral Analysis of Polymer Transition Temperatures. Journal of Physical Chemistry B, 2008, 112, 3611-3616.	2.6	16
102	Density control of ZnO nanowires grown using Au-PMMA nanoparticles and their growth behavior. Nanotechnology, 2009, 20, 085601.	2.6	16
103	Hydrogen-Bonding Networks of Dialkyl Disulfides Containing the Urea Moiety in Self-Assembled Monolayers. Langmuir, 2004, 20, 1674-1679.	3.5	15
104	Large-Area Hexagonal Boron Nitride Layers by Chemical Vapor Deposition: Growth and Applications for Substrates, Encapsulation, and Membranes. Accounts of Materials Research, 2022, 3, 748-760.	11.7	13
105	Spontaneous electron transfer from C60 to Au ions: oxidation of C60 and hole doping. Journal of Materials Chemistry, 2010, 20, 7183.	6.7	12
106	Superstructural defects and superlattice domains in stacked graphene. Carbon, 2014, 80, 755-761.	10.3	12
107	Sphereâ€ŧoâ€Multipod Transmorphic Change of Nanoconfined Pt Electrocatalyst during Oxygen Reduction Reaction. Small, 2019, 15, e1802228.	10.0	12
108	Mechanical Properties of Poly(dopamine)â€Coated Graphene Oxide and Poly(vinyl alcohol) Composite Fibers Coated with Reduced Graphene Oxide and Their Use for Piezoresistive Sensing. Particle and Particle Systems Characterization, 2017, 34, 1600382.	2.3	11

#	Article	IF	CITATIONS
109	Anomalous Ambipolar Transport of Organic Semiconducting Crystals via Control of Molecular Packing Structures. ACS Applied Materials & Interfaces, 2017, 9, 27839-27846.	8.0	10
110	Strong exciton-photon coupling in large area MoSe2 and WSe2 heterostructures fabricated from two-dimensional materials grown by chemical vapor deposition. 2D Materials, 2021, 8, 011002.	4.4	10
111	Effect of Pt Crystal Surface on Hydrogenation of Monolayer h-BN and Its Conversion to Graphene. Chemistry of Materials, 2020, 32, 4584-4590.	6.7	9
112	Synthesis of 1T WSe <sub>2</sub> on an Oxygen-Containing Substrate Using a Single Precursor. ACS Nano, 2022, 16, 11059-11065.	14.6	9
113	Spatially controlled lateral heterostructures of graphene and transition metal dichalcogenides toward atomically thin and multi-functional electronics. Nanoscale, 2020, 12, 5286-5292.	5.6	8
114	Radio-frequency-transmitting hexagonal boron nitride-based anti- and de-icing heating system. Nanoscale, 2020, 12, 21895-21900.	5.6	7
115	Quantum Efficiency Enhancement of Bialkali Photocathodes by an Atomically Thin Layer on Substrates. Physica Status Solidi (A) Applications and Materials Science, 2019, 216, 1900501.	1.8	6
116	Improving Radio Frequency Transmission Properties of Graphene via Carrier Concentration Control toward High Frequency Transmission Line Applications. Advanced Functional Materials, 2019, 29, 1808057.	14.9	6
117	Interlayer electron modulation in van der Waals heterostructures assembled by stacking monolayer MoS <sub>2</sub> onto monolayer graphene with different electron transfer ability. Nanoscale, 2021, 13, 15464-15470.	5.6	6
118	Selective formation of thickness-controlled fullerene disks by vapor–solid process. Journal of Crystal Growth, 2013, 363, 141-144.	1.5	4
119	Functionalized graphene sheets/polycarbonate nanocomposites compatibilized by poly(phenylenevinylene). Macromolecular Research, 2012, 20, 768-771.	2.4	3
120	Toward growth of wafer-scale single-crystal hexagonal boron nitride sheets. Nano Express, 2021, 2, 031004.	2.4	3
121	Synthesis of metallic mixed 3R and 2H Nb <sub>1+x</sub> S <sub>2</sub> nanoflakes by chemical vapor deposition. Faraday Discussions, 2021, 227, 332-340.	3.2	2
122	Reply to: On the measured dielectric constant of amorphous boron nitride. Nature, 2021, 590, E8-E10.	27.8	1
123	Phase- and composition-controlled synthesis. Nature Materials, 0, , .	27.5	1
124	Radio Frequency Transmission: Improving Radio Frequency Transmission Properties of Graphene via Carrier Concentration Control toward High Frequency Transmission Line Applications (Adv. Funct.) Tj ETQq0 0 0 (	rg <b>B4.</b> ¢Ovei	look 10 Tf 50

125	Dendritic Multipods: Sphere-to-Multipod Transmorphic Change of Nanoconfined Pt Electrocatalyst during Oxygen Reduction Reaction (Small 2/2019). Small, 2019, 15, 1970013.	10.0	0	
-----	---	------	---	--